

Nuclear cross sections from low-energy interactions

J. Boström, J. Rotureau, B. G. Carlsson, and A. Idini
*Division of Mathematical Physics, Department of Physics, LTH,
Lund University, PO Box 118, S-22100 Lund, Sweden*

We present a method to calculate neutron scattering cross sections for deformed nuclei using many-body wavefunctions described with multiple reference states. Nuclear states are calculated with the generator coordinate method using a low energy effective Hamiltonian. Using these states, a non-local and energy dependent optical potential is consistently constructed, allowing to directly investigate the role of nuclear structure properties in nuclear scattering. The case of neutron scattering on ^{24}Mg is presented. The results are compared to experiment and to phenomenological optical potentials at energies below 13 MeV, demonstrating the importance of low-energy collectivity in elastic and non-elastic scattering.

INTRODUCTION

Nuclear reactions are one of the fundamental methods used to study and understand atomic nuclei. Exotic nuclei, which must be produced in radioactive ion beam facilities and studied before they decay, are often investigated through reaction processes [1, 2]. Reactions are not only crucial for understanding nuclei but also play a significant role in various astrophysical phenomena, such as stellar burning and nucleosynthesis [3, 4].

It is extremely challenging to study nuclear reactions using state-of-the-art nuclear structure information in a consistent framework. The complexity of the dynamical processes happening during a scattering process often forces the use of separate and inconsistent models of structure and reaction, frequently relying on phenomenological optical potentials [5, 6]. Optical potentials represent the effective interaction between projectile and target and they are an effective way to decouple internal degrees of freedom and reaction dynamics [7]. They can be calculated exactly from the Hamiltonian of the many-body problem projected onto the elastic scattering channel, as shown already in [8]. Recently, several efforts have been made to calculate cross sections and produce adequate optical potential consistently using microscopic nuclear structure models from Hamiltonian projection (cf. [1, 9] and refs. therein).

It is additionally difficult to describe reactions involving deformed nuclei. The symmetry breaking mechanisms that efficiently describe the deformation, impose an additional complexity to both the formalism and the computation of nuclear properties and their application to reactions [10].

In this manuscript, we propose a novel method for constructing an optical potential for deformed nuclei using microscopic symmetry breaking and restoration calculations. The formalism needed to construct Green's functions and corresponding self-energy from multiple reference states is presented. This method is then used to calculate scattering cross sections of $n+^{24}\text{Mg}$.

Our approach builds on previous work utilizing the

generator coordinate method (GCM) with an effective low-energy interaction [11]. This combination is a versatile many-body framework capable of describing both light and superheavy deformed nuclei [11–13].

The present study investigates the role of many-body correlations in scattering, with a particular focus on whether low-energy collectivity contributes to the observed elastic scattering cross sections. In [14] self-consistent Green's functions were used to calculate neutron elastic scattering of ^{16}O and ^{40}Ca , noting that the overestimation of elastic scattering cross section was due to lacking correlations and collectivity. With this method we overcome this issue, concluding that GCM is suitable to reproduce the low-energy collectivity important for reaction properties. These results show a promising route towards the systematic construction of microscopic optical for heavy and deformed nuclei.

METHOD

We employ a Hamiltonian $\hat{H} = E_0 + \hat{\Gamma} + \hat{V}$, where E_0 is a constant, $\hat{\Gamma}$ and \hat{V} are the one and two-body components respectively. The form may be derived starting from a general interaction by a normal ordering procedure that approximates the three-body interaction [15]. In our case, the terms are given by a low-energy effective Hamiltonian that captures the response of an energy density functional to external fields [11].

The many-body basis that is used to solve the Hamiltonian consists of Hartree-Fock-Bogoliubov (HFB) vacua varied over a set of generator coordinates. The collective coordinates that generate the GCM basis are the familiar β , and γ for quadrupole deformation and triaxiality, in addition to a variation of the neutron-proton pairing fields scaled by g_n, g_p factors, and different cranking constraint j_x . Each HFB state $|\Phi(\beta, \gamma, g_n, g_p, j_x)\rangle$ will then be excited with a Bogoliubov singles coupled cluster operator with a temperature-like weighting obtaining $|\Phi_x\rangle$ [11]. This choice of generator coordinates and reference states accounts for the most important degrees of freedom of single-particle, collective vibrations, rota-

tions and pairing vibrations already within the reference states. Additionally, to describe states with an odd number of particles, we apply the quasiparticle creation operator β_a^\dagger to each HFB reference state, $|\Phi_{a,x}^\pm\rangle = \beta_a^\dagger |\Phi_x\rangle$.

These basis states are then projected to good angular momenta and particle numbers to calculate Hamiltonian and overlap matrices. The Hill–Wheeler equation is then constructed and solved, finally obtaining states $|\Psi_i^{\pm J\pi}\rangle = \sum_{a,x,M} h_{a,x,i,M}^{J\pi} P_{K,M}^J P_Z P_{N\pm 1} |\Phi_{a,x}^\pm\rangle$, where Ψ_i^\pm denote states with $A \pm 1$ particles with energy E_i^\pm , and Ψ_i denotes a state with A particles with energy E_i . J is the total angular momentum, $\pi = \pm 1$ is the parity, i the label of the state, $h_{a,x,i}^{J\pi}$ are coefficients, and $P_{M,K}^J$ and P_A are the projection operators for angular momentum and particle number respectively. The method and the effective Hamiltonian used are described in detail in [11].

Spectroscopic amplitudes

Using the GCM wavefunctions, we then calculate the spectroscopic amplitudes of the odd–even states with respect to the even–even ground state Ψ_0 , defined as $s_{i,\alpha}^{+J\pi} \equiv \langle \Psi_i^{+J\pi} | a_\alpha^\dagger | \Psi_0 \rangle$ and $s_{i,\alpha}^{-J\pi} \equiv \langle \Psi_0 | a_\alpha^\dagger | \Psi_i^{-J\pi} \rangle$, where a_α^\dagger is the particle creation operator which creates a particle in the state α in m-scheme. The spectroscopic amplitudes represent how well the states $|\Psi_i^{\pm J\pi}\rangle$ are described as a single particle in the state α added on (or removed from) the even ground state Ψ_0 . Their absolute squares, $|s|^2$, are called spectroscopic factors. Since the single particle states α are basis dependent, the spectroscopic amplitudes are not directly observable in experiments.

When calculating using a spherically symmetric single–particle basis, and since the even–even ground state will have spin 0 and positive parity, the spectroscopic amplitude is only non–zero when the spin and parity of the state α matches the spin and parity of the odd–even state $\Psi_i^{+J\pi}$, so $J_\alpha = J$ and $\pi_\alpha = \pi$, and it’s only necessary to project the ket [16, 17]. More information regarding the calculation of the spectroscopic factors can be found in [18, 19].

Completion

The spectroscopic amplitudes must fulfil the following sum rule for each $J\pi$ shell, $\sum_{i,x=\pm} (s_{i,\alpha}^{+J\pi})^* s_{i,\beta}^{+J\pi} = \delta_{\alpha,\beta}$. Furthermore, it exists an energy weighted sum rule for the spectroscopic amplitudes,

$$\sum_{i,x=\pm} (s_{i,\alpha}^{+J\pi})^* \bar{E}_i^{J\pi} s_{i,\beta}^{+J\pi} = \langle \Psi_0 | \left\{ a_\alpha, \left[\hat{H}, a_\beta^\dagger \right] \right\} | \Psi_0 \rangle, \quad (1)$$

with $\bar{E}_i^{\pm J\pi} = \pm \left(E_i^{\pm J\pi} - E_0 \right)$, which is related to the spectroscopic sum rule derived for nuclear matter in [20]. The GCM solutions are calculated independently in the Hilbert spaces of A and $A \pm 1$ particles, and will not automatically form a complete basis of the considered Fock space.

In order to fulfill the sum rules in the very large Fock spaces spanned by our calculations we complete the spectroscopic amplitudes by introducing additional amplitudes $c_{k,\alpha}^{J\pi}$ and energies $\epsilon_k^{J\pi}$, such that they satisfy the sum rules in the following way,

$$\begin{aligned} \sum_{i,x=\pm} (s_{i,\alpha}^{+J\pi})^* s_{i,\beta}^{+J\pi} + \sum_{k=1}^{N^{J\pi}} (c_{k,\alpha}^{J\pi})^* c_{k,\beta}^{J\pi} &= \delta_{\alpha,\beta}, \quad (2) \\ \sum_{i,x=\pm} (s_{i,\alpha}^{+J\pi})^* \bar{E}_i^{J\pi} s_{i,\beta}^{+J\pi} + \sum_{k=1}^{N^{J\pi}} (c_{k,\alpha}^{J\pi})^* \epsilon_k^{J\pi} c_{k,\beta}^{J\pi} \\ &= \sum_{k=1,x=\pm}^{N^{J\pi}} (s_{k,\alpha}^{0x J\pi})^* E_k^{0x J\pi} s_{k,\beta}^{0x J\pi}. \quad (3) \end{aligned}$$

Here we have approximated the many–body ground state $|\Psi_0\rangle$ in Eq. (1) with the spherical Hartree–Fock (HF) ground state, $N^{J\pi}$ is the number of shells with the given spin and parity, $s_{k,\alpha}^{0\pm J\pi}$ are the spectroscopic amplitudes of the HF solution, and $E_k^{0\pm J\pi}$ are the single particle energies of the HF solution.

In the case where the solutions from GCM fulfill the sum rules, the added $c_{k,\alpha}^{J\pi}$ go to zero and $\epsilon_k^{J\pi}$ go to infinity, and so the the GCM solution would completely determine the properties in the energy range of interest. On the other hand, if the GCM procedure would fail to find any state, the additional spectroscopic amplitudes and energies would be the same as in the HF case.

Optical potential

The completed spectroscopic amplitudes and energies are then used to calculate an optical potential using the Green’s function formalism.

The unperturbed propagator $G_0(E)$ represents the propagation of a particle in an external potential or a free particle, while the dressed propagator $G(E)$ considers the effect of the interaction of the particle with a many–body system. The two are related through the self energy $\Sigma(E)$ and the Dyson equation $G(E) = G_0(E) + G_0(E) \Sigma(E) G(E)$.

We define the Green’s function in the Källén–Lehmann representation using Eq. (2,3) as,

$$G_{\alpha,\beta}^{J\pi}(E) = \sum_{i,x=\pm} \frac{(s_{i,\alpha}^{+J\pi})^* s_{i,\beta}^{+J\pi}}{E - \bar{E}_i^{J\pi}(\eta)} + \sum_k \frac{(c_{k,\alpha}^{J\pi})^* c_{k,\beta}^{J\pi}}{E - \bar{\epsilon}_k^{J\pi}(\eta)}, \quad (4)$$

where $\bar{E}_i^{\pm J\pi}(\eta) = \pm \left(E_i^{\pm J\pi} - E_0 - i\eta \right)$ and η is a term to avoid the poles at the excitation energies ensuring causality. $\bar{\epsilon}_k^{J\pi}(\eta)$ is chosen as $\bar{\epsilon}_k^{J\pi}(\eta) = \epsilon_k^{J\pi} + i\eta$ for $\epsilon_k^{J\pi} < E_F$ and $\bar{\epsilon}_k^{J\pi}(\eta) = \epsilon_k^{J\pi} - i\eta$ for $\epsilon_k^{J\pi} > E_F$, where E_F can be set appropriately according to the French-McFarlane sum rules [19, 21] but it can be taken as the Fermi energy $(E_0^+ - E_0^-)/2$ with no difference to the results presented here. Due to the rotational and reflection symmetries of the Hamiltonian, the Green's function are in separate $J\pi$ blocks. We construct the $G_0^{J\pi}(E)$ using the Hartree-Fock solution, substituting in Eq. (4) $s_{i,\alpha}^{x,J\pi}$ with $s_{i,\alpha}^{0x,J\pi}$, $\bar{E}_i^{\pm J\pi}(\eta)$ with $E_i^{0x,J\pi} \mp i\eta$, and $c_{k,\alpha}^{J\pi}$ with 0.

The Dyson equation can be solved for $\Sigma^{J\pi}$ as

$$\Sigma^{J\pi}(E) = (G_0^{J\pi}(E))^{-1} - (G^{J\pi}(E))^{-1}. \quad (5)$$

The total potential is then the sum of the static Hartree-Fock potential $U_0^{J\pi}$, that defined the unperturbed solution, and the self energy,

$$V^{J\pi}(E) = U_0^{J\pi} + \Sigma^{J\pi}(E), \quad (6)$$

and it is by construction an energy dependent, non-local, and dispersive optical potential. The completion procedure of Eq. (2,3) has been defined so that $\Sigma^{J\pi}(E) \rightarrow 0$ for $E \rightarrow \infty$ reducing to the Hartree-Fock potential and corresponding propagator in absence of a GCM solution at the relevant energy.

In our calculations, $V^{J\pi}(E)$ is first expressed in a finite harmonic oscillator basis. When transforming to momentum basis, a smoothing factor

$$\sigma_n = \frac{1 - \exp\left(-\left(\alpha \frac{n-N^{J\pi}}{N^{J\pi}}\right)^2\right)}{1 - \exp(-\alpha^2)} \quad (7)$$

is applied to the matrix elements, where α is a dimensionless parameter as in [22] ($\alpha = 5$). This smoothing factor improves convergence by decreasing the effect of the basis truncation [23, 24]. Then, the potential in momentum space becomes,

$$V^{J\pi}(p, p', E) = \sum_{\alpha, \beta} \phi_\alpha(p) \sigma_\alpha V_{\alpha, \beta}^{J\pi}(E) \sigma_\beta \phi_\beta(p')^*, \quad (8)$$

where ϕ_n are the radial harmonic oscillator wavefunctions in momentum space. The momentum space Schrödinger equation describing the scattering neutron of energy E_{cm} in the center of mass frame for a given partial wave is

$$\frac{p^2}{2\mu} u(p) + \gamma^3 \int dp' p'^2 V^{J\pi}(\gamma p, \gamma p', \gamma E_{\text{cm}}) u(p') = E_{\text{cm}} u(p), \quad (9)$$

where $\gamma \equiv m_1/\mu = 1 + 1/A$, $\mu = m_1 m_2 / (m_1 + m_2)$ is the reduced mass, m_1 and m_2 are the projectile and target masses [14]. The Schrödinger equation in the laboratory

frame is obtained substituting the reduced mass with the projectile mass, γ with 1, and E_{cm} with the projectile energy in the laboratory frame E_p .

This Schrödinger equation is then solved using the Lippmann-Schwinger equation in momentum space, giving the phase shifts for each partial wave, $\delta_{J\pi}$. The phase shifts are then used to calculate differential cross sections $d\sigma/d\Omega$, as well as integrated elastic, reaction, and total cross sections σ_E , and σ_T , in the same way as in [25].

RESULTS

$^{24}\text{Mg} + n$ scattering

As the first implementation of this method, we have calculated total and elastic neutron scattering cross sections of the characteristically prolate deformed nucleus ^{24}Mg .

Following the procedure described in [11], the effective Hamiltonian was created using the SLy4 Skyrme parameterization. The number of major shells in the harmonic oscillator single-particle basis was 17 in the HF calculation, but the 586 lowest energy HF states (which correspond to approximately as many states as there would be in 11 major shells) were used as the single-particle basis for the GCM. We then sampled the $\beta\gamma$ plane with 275 states. Keeping states below 25 MeV resulted in 179 HFB basis states. The states were projected with 10 particle number projection points, and (6, 12, 24) angular momentum projection points for the (α, β, γ) angles and $b = 0.45$. The odd-even HFB basis consisted of one quasiparticle excitation for each even-even HFB state. The quasiparticle to excite was chosen randomly among the 10 quasiparticles with the lowest mean-field energy of a given signature and $J\pi$ such that quasiparticle states that correspond to the wrong particle number are also excluded, i.e. hole states when calculating the solution for $A + 1$. These parameters were chosen to ensure optimal convergence in the energy range presented. Using this Hamiltonian and basis states, the states of $^{23,24,25}\text{Mg}$ were calculated [11, 18]. The wavefunctions were then used to calculate the spectroscopic amplitudes of ^{23}Mg and ^{25}Mg relative to the ground state of ^{24}Mg .

Then, for the scattering calculations, η was set to $\eta = \frac{a}{\pi} \frac{(E-E_f)^2}{(E-E_f)^2 + b^2}$ with $a = 12$ MeV and $b = 22.36$ MeV as in [26].

The cross sections are calculated for the two signatures $\pm i$. The signature is a preserved symmetry and should not have effect on observables in an exact calculation, but due to the random selection of basis states and quasiparticle excitation in the GCM, and the inclusion of cranking, quasiparticle states of different signature behave differently [29]. Comparing the two can give an indication of the convergence of the GCM calculation.

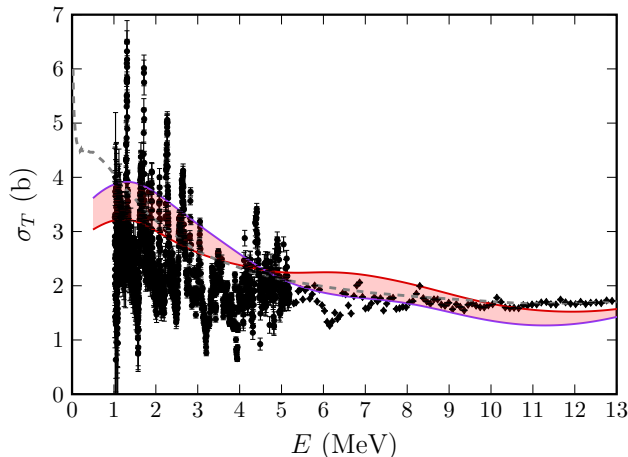


Fig. 1. The total scattering cross section of $^{24}\text{Mg} + n$ in function of the neutron energy. The red and purple lines correspond to the cross sections calculated using the method described in this paper with signature $+i$ and $-i$ respectively and the area between them is shaded red. The dashed line are result using the Koning–Delaroche optical potential. The black circles are experimental cross sections for ^{24}Mg [27], while the diamonds are natural Magnesium [28].

In Fig. 1 the integrated neutron total cross sections are shown for energies from $E = 0.5$ MeV to 13 MeV, together with the result of Koning–Delaroche optical potential [5]. We can see a good agreement with experimental data for the whole region, and the phenomenological Koning–Delaroche results lie in the middle of our predicted interval for most of the region below 10 MeV. Due to the choice of η , resonances are wider than what experiments show at low energies.

The elastic scattering cross section is also calculated and compared to experiment in Fig. 2. We see that the calculated cross section reproduces experiments up to 9 MeV, but overestimates them for neutron energies above 10 MeV. This indicates that the method fails to find enough states that contribute to the non-elastic channels above 9 MeV, and progressively more of the contribution comes from the HF solution through the completion. The static HF potential is real and only the elastic scattering channel is available in this case, resulting in a sizeable overestimation of the elastic scattering cross section in Fig. 2. At higher energy the calculated GCM $\sigma_{E,T}$ will gradually reach the HF result above 20 MeV.

The angular differential cross sections were calculated for several projectile energies shown in Fig. 3, together with the corresponding experimental values. We see also for the differential cross section a general agreement with experiment. For some energies this method underestimates the cross section at the minima, which could be due to an underestimation of the compound nucleus reaction channels. This is when the neutron is absorbed

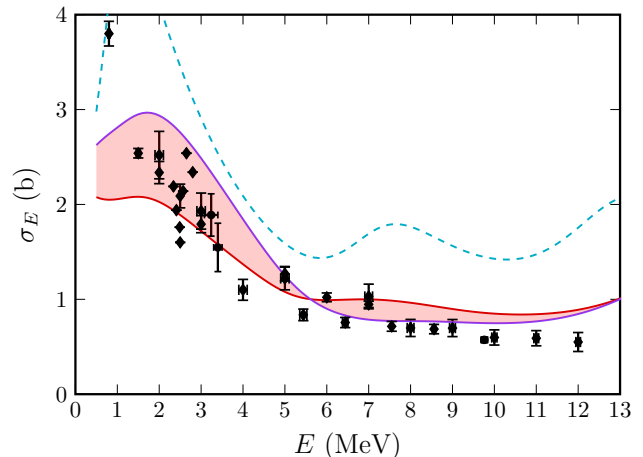


Fig. 2. The elastic scattering cross section of $^{24}\text{Mg} + n$ in function of neutron energy. The lines and datapoints mean the same as in Fig. 1. Additionally, the integrated cross section calculated with only the HF potential is shown as a dashed blue line. The experimental cross sections for ^{24}Mg are from [30–32], while the natural Magnesium cross sections are from [33–40].

and an excited ^{25}Mg is formed. This compound nucleus will then decay and one possible decay mode is to emit a neutron. If the emitted neutron has the same energy as the original incoming neutron, the result is identical to elastic scattering. Since the compound nucleus has time to thermalize, the emission is isotropic and it will contribute an angle independent term to the differential cross section. The compound nucleus contribution is expected to be larger at lower energies, and in Fig. 3 the results at lower neutron energies can be seen to underestimate the minima in the experimental cross sections. The effect of the compound nucleus are particularly challenging to model from a Hamiltonian and is under further investigation [42].

In conclusion, we have found that the lack of absorption observed when using a microscopically generated optical potential, that was linked to configurations beyond particle–hole excitation in [14], is properly taken into account through the collective degrees of freedom when using GCM. This shows that GCM captures the necessary low energy correlations needed to accurately describe low energy neutron scattering to a level that was not previously achieved. This work extends microscopic reaction approaches to study deformed, heavy, and exotic nuclei, representing a significant step towards a unified model of nuclear structure and reaction.

ACKNOWLEDGEMENTS

This work has been supported by the Swedish Research Council (Vetenskapsrådet) VR 2020-03721, Knut and

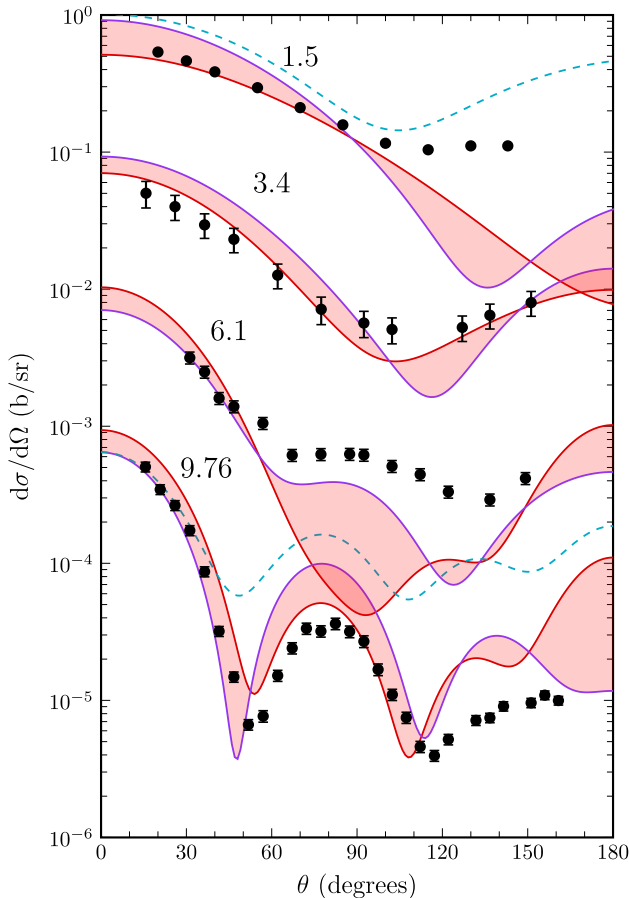


Fig. 3. The differential cross section of elastic $^{24}\text{Mg} + n$ scattering for four different neutron energies. The energies are shown in the figure in MeV. The lines and datapoints mean the same as in Fig. 2. The dashed line refer to the HF calculation at 1.5 and 9.76 MeV. The experimental data are from [30, 31, 35, 41]. The 1.5 MeV reaction is represented in laboratory frame, while the other energies are represented in center of mass frame. The cross sections for each energy are shifted down by a factor of 10 relative to the previous.

Alice Wallenberg foundation (KAW 2015.0021), Craford foundation, and Krapperup foundation. Computing was enabled by resources provided by the National Academic Infrastructure for Supercomputing in Sweden (NAISS), partially funded by the Swedish Research Council through grant agreement no. 2022-06725, and The Centre for Scientific and Technical Computing at Lund University (LUNARC).

[1] C. W. Johnson, K. D. Launey, and others, *Journal of Physics G: Nuclear and Particle Physics* **47**, 123001 (2020).
 [2] H. Crawford, K. Fosse, S. König, and A. Spyrou, *Annual Review of Nuclear and Particle Science* **74** (2024).

[3] F. Nunes, *Nucl. Phys. A* **757**, 349 (2005).
 [4] H. Schatz and et al., *Journal of Physics G: Nuclear and Particle Physics* **49**, 110502 (2022).
 [5] A. J. Koning and J. P. Delaroche, *Nucl. Phys. A* **713**, 231 (2003).
 [6] C. D. Pruitt, J. E. Escher, and R. Rahman, *Phys. Rev. C* **107**, 014602 (2023).
 [7] H. Feshbach, *Annual Review of Nuclear Science* **8**, 49 (1958).
 [8] H. Feshbach, *Annals of Physics* **5**, 357 (1958).
 [9] C. Hebborn, F. M. Nunes, G. Potel, *et al.*, *J. Phys. G* **50**, 060501 (2023).
 [10] A. Idini *et al.*, *J. Phys.: Conf. Ser.* **2586**, 012049 (2023).
 [11] J. Ljungberg, B. G. Carlsson, J. Rotureau, A. Idini, and I. Ragnarsson, *Phys. Rev. C* **106**, 014314 (2022).
 [12] A. Sămark-Roth *et al.*, *Phys. Rev. Lett.* **126**, 032503 (2021).
 [13] J. Ljungberg *et al.*, *J. Phys.: Conf. Ser.* **2586**, 012081 (2023).
 [14] A. Idini, C. Barbieri, and P. Navrátil, *Phys. Rev. Lett.* **123**, 092501 (2019).
 [15] W. Lin, E. Zhou, J. Yao, and H. Hergert, *Symmetry* **16**, 10.3390/sym16040409 (2024).
 [16] H.-B. Håkansson, T. Berggren, and R. Bengtsson, *Nuclear Physics A* **306**, 406 (1978).
 [17] K. Enami, K. Tanabe, and N. Yoshinaga, *Phys. Rev. C* **59**, 135 (1999).
 [18] J. Boström *et al.*, *J. Phys.: Conf. Ser.* **2586**, 012080 (2023).
 [19] J. Boström, B. G. Carlsson, and A. Idini, To be published.
 [20] A. Polls, A. Ramos, J. Ventura, S. Amari, and W. H. Dickhoff, *Phys. Rev. C* **49**, 3050 (1994).
 [21] Supplementary Material.
 [22] W. Du, S. Pal, M. Sharaf, P. Yin, S. Sarker, A. M. Shirokov, and J. P. Vary, *Phys. Rev. C* **106**, 054608 (2022).
 [23] J. Revai, M. Sotona, and J. Zofka, *J. Phys. G: Nucl. Phys.* **11**, 745 (1985).
 [24] A. M. Shirokov, A. I. Mazur, and V. A. Kulikov, *Physics of Atomic Nuclei* **84**, 131 (2021).
 [25] H. Arellano and G. Blanchon, *Computer Physics Communications* **259**, 107543 (2021).
 [26] S. Waldecker, C. Barbieri, and W. H. Dickhoff, *Phys. Rev. C* **84**, 034616 (2011).
 [27] J. Bommer, M. Ekpo, H. Fuchs, K. Grabisch, and H. Kluge, *Nuclear Physics A* **263**, 86 (1976).
 [28] W. P. Abfalterer, F. B. Bateman, F. S. Dietrich, R. W. Finlay, R. C. Haight, and G. L. Morgan, *Phys. Rev. C* **63**, 044608 (2001).
 [29] B. Bally and M. Bender, *Phys. Rev. C* **103**, 024315 (2021).
 [30] A. Viridis, Rept: Centre d'Études Nucleaires, Saclay Reports, 5144 (1981).
 [31] T. Schweitzer, D. Seeliger, and S. Unholzer, EXFOR30463 (1978).
 [32] L. Frittelli, F. Vinci, and E. Demanins, Rept: Com.Naz. per l'Energia Nucleare Reports (1970).
 [33] I. Korzh, V. Mishchenko, N. Pravdivy, and N. Sklyar, *Ukrainskii Fizichnii Zhurnal* **39**, 785 (1994).
 [34] M. Adel-Fawzy, H. Förtisch, D. Schmidt, D. Seeliger, and T. Streil, *Nuclear Physics A* **440**, 35 (1985).
 [35] I. Korzh, V. Mishchenko, M. Pasechnik, N. Pravdivyi, I. Sanzhur, and I. Totksii, *Ukrainian Physics Journal* **13**,

- 1266 (1969).
- [36] I. Korzh, N. Kopytin, M. Pasechnik, N. Pravdivyi, N. Sclyar, and I. Totskii, *Soviet Atomic Energy* **16**, 312 (1964).
- [37] I. Korzh and N. Sklyar, *Ukrainskii Fizichnii Zhurnal* **8**, 1389 (1963).
- [38] D. B. Thomson, L. Cranberg, and J. S. Levin, *Phys. Rev.* **125**, 2049 (1962).
- [39] R. N. Little, R. W. Long, and C. E. Mandeville, *Phys. Rev.* **69**, 414 (1946).
- [40] M. R. MacPhail, *Phys. Rev.* **57**, 669 (1940).
- [41] D. Stewart, W. Currie, J. Martin, and P. Martin, *Conf: Nuclear Structure Study with Neutrons*, Antwerp , 509 (1965).
- [42] G. H. Sargsyan, G. Potel, K. Kravvaris, and J. E. Escher, *Microscopic optical potentials from a greens function approach* (2024), arXiv:2410.21714 [nucl-th].